Chemosphere 291 (2022) 132702

Contents lists available at ScienceDirect

Chemosphere

journal homepage: www.elsevier.com/locate/chemosphere

Hierarchical porous structure formation mechanism in food waste component derived N-doped biochar: Application in VOCs removal

Yuxuan Yang, Chen Sun, Qunxing Huang *, Jianhua Yan

State Key Laboratory of Clean Energy Utilization, Zhejiang University, Hangzhou, 310027, China

HIGHLIGHTS

- N-doped hierarchical porous biochar was prepared from direct pyrolysis process.
- The combined self-activation and self-templated effect was studied.
- CO_2 generation had an exclusive influence on micropores' production.
- N-doped hierarchical porous biochar could remove toluene effectively (288 mg/g).

GRAPHICAL ABSTRACT

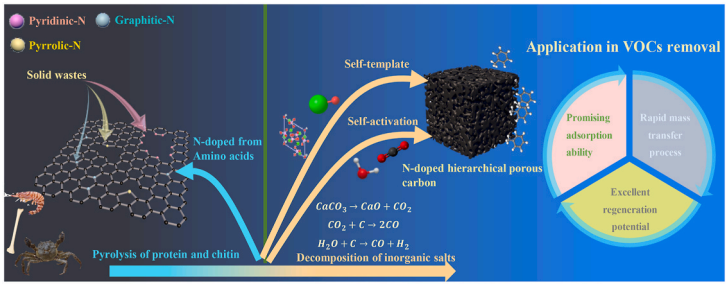

ARTICLE INFO

Handling Editor: Chang-Ping Yu

Keywords:
Nitrogen-doped
Hierarchical porous carbon
Food waste
VOCs adsorption

ABSTRACT

Nitrogen-doped (N-doped) hierarchical porous carbon was widely utilized as an efficient volatile organic compounds (VOCs) adsorbent. In this work, a series of N-doped hierarchical porous carbons were successfully prepared from the direct pyrolysis process of three food waste components. The porous biochar that derived from bone showed a high specific surface area (1405.06 m^2/g) and sizable total pore volume (0.97 cm^3/g). The developed hierarchical porous structure was fabricated by the combined effect of self-activation (Carbon dioxide (CO_2) and water vapor (H_2O)) and self-template. The emission characteristics of activation gas analyzed by Thermogravimetric-Fourier transform infrared spectrometer (TG-FTIR) and the transformation of ash composition in the biochar help to illustrate the pore-forming mechanism. Calcium oxide (CaO) and hydroxylapatite were confirmed as the major templates for mesopores, while the decomposition processes of calcium carbonate ($CaCO_3$) and hydroxylapatite provided a large amount of activation gas (CO_2 and H_2O) to form micropores. The materials also obtained abundant N-containing surface functional groups (up to 7.84 atomic%) from pyrolysis of protein and chitin. Finally, the porous biochar showed excellent performance for VOCs adsorption with a promising uptake of 288 mg/g for toluene and a high adsorption rate of 0.189 min^{-1}. Aplenty of mesopores distributed in the materials effectively improved the mass transfer behaviors, the adsorption rate got a noticeable improvement (from 0.118 min^{-1} to 0.189 min^{-1}) benefited from mesopores. Reusable potentials of the hierarchical porous carbons were also satisfying. After four thermal regeneration cycles, the materials still occupied 84.8%–87.4% of the original adsorption capacities.

* Corresponding author.
E-mail address: hqx@zju.edu.cn (Q. Huang).

https://doi.org/10.1016/j.chemosphere.2021.132702
Received 15 June 2021; Received in revised form 2 September 2021; Accepted 24 October 2021
Available online 25 October 2021

1. Introduction

VOCs generated from energy conversion (Yan et al., 2016), solid waste disposal (Nie et al., 2018), and building decoration processes (Gao et al., 2021) were harmful to human health. Adsorption by carbon-based materials is currently the most widely utilized, low-cost, and efficient emission control method (Zhang et al., 2017). Traditional carbon-based materials including activated carbon (Bedane et al., 2019), biochar (Xiang et al., 2020), carbon nanotubes (CNTs) (Crespo and Yang, 2006), graphene (Chabot et al., 2014), carbon-silica composites (Janus et al., 2011), etc., were reported as efficient VOCs adsorbents.

With rapid economic development and population growth, plant-based and animal-based food waste is generated increasingly (Li et al., 2019). Over 300 million tons of animal meat (from livestock, poultry, and fish) are produced per year around the world (Sharma et al., 2015). Meanwhile, abundant byproducts including bone, crab shell, and shrimp shell generated. As previous literature reported (León et al., 2019), in the European Union (EU), the over 20 million tons that are being generated annually emerge from slaughterhouses, plants producing food for human consumption, dairies, and fallen stock from farms. The reduction and reuse of the food waste components are urgent needs.

Nowadays, biochar prepared from food waste components and its processing byproducts was reported as potential VOCs adsorbents. Rajabi et al., (2021) prepared valuable biochar from wheat straw and bagasse sugarcane for VOCs removal. The biochar showed satisfying adsorption performances for various VOCs species (51–110 mg/g). Jin et al., (2020) successfully prepared air pre-oxidation biochar from stillage. The materials showed a promising toluene removal amount (437.8 mg/g).

Importing heteroatom into the hierarchical porous carbon was an efficient surface modification method to enhance the interactions between materials' surfaces and target adsorbate molecules. N-containing functional groups can enhance the adsorption effect by increasing the polarity of materials' surfaces (Ma et al., 2019). Lu et al., (2021) synthesized N-doped hierarchical porous carbon with an excellent toluene adsorption capacity (585 mg/g) from cellulose by one-step activation and modification with ammonium oxalate $(NH_4)_2C_2O_4$ and potassium bicarbonate ($KHCO_3$)/sodium bicarbonate ($NaHCO_3$). Pi et al., (2021) prepared N-doped hierarchical porous wood char, which was activated and modified by ammonia water. The material can effectively remove VOCs (54.9 mg/g for dichloromethane and 308 mg/g for toluene).

Hierarchical porous carbon with high specific surface area, large total pore volume, and tailored pore structures were widely utilized as VOCs adsorbents (Sun et al., 2016). Compared to traditional microporous carbon materials, hierarchical porous carbon exhibited superior mass transfer potential which can lead to a more efficient adsorption process (Tang et al., 2020; Yang et al., 2020, 2021). Usually, to obtain materials with high specific surface area and hierarchical porous structure from solid wastes, physical or chemical activation process was necessary. Eco-friendly self-activation by using released gases (CO_2 and H_2O, etc.) from the carbonization process as the activation agent can effectively simplify the preparation procedure and reduce the extra cost. Bommier et al., (2015) reported that activated carbon with a high specific surface area (2602 m^2/g) could be prepared from direct high-temperature pyrolysis of cellulose. The self-activation agent H_2O was evolved in situ during the pyrolysis process over a wide range of temperatures. Sun et al., (2017) prepared coconut shell-based activated carbon by self-activation using CO_2 generated from the pyrolysis process. They also proved that almond stone, pecan shell, and slash pine sawdust were also appropriate raw materials for the self-activation process. Gao et al., (2018) successfully synthesized a 2D hierarchical porous carbon sheet from the soft pitch and oyster shell by self-activation and templating effect. Calcite embed in the oyster shell played the role of template and activation agent.

Based on the above analysis, N-doped hierarchical porous biochar prepared from direct pyrolysis of food waste components is considered as a low-cost, interesting, and satisfying VOCs adsorbent. Animal-based food waste byproducts including bone and seafood shells are appropriate raw materials for N-doped hierarchical porous biochar. Abundant protein provided enough nitrogen and inorganic salts played the role of templates during the hierarchical porous pore-forming process (Niu et al., 2019). Meanwhile, the thermal conversion process can realize the reduction and reuse of food wastes. However, the pyrolysis process and pore-forming mechanisms of animal-based food waste byproducts were rarely reported. Therefore, it is essential to study the pyrolysis process and develop a preparation method from animal-based food waste byproducts that can directly obtain high-quality materials in the thermal conversion process.

Herein, we selected three nitrogen and inorganic salts-enriched food waste components (bone, crab shell, and shrimp shell) as raw materials for N-doped hierarchical porous carbon. Through direct high-temperature pyrolysis (700 °C–900 °C) and acid etching, a series of N-doped carbon with the developed porous structure were prepared. The materials' porous structures were characterized by N_2 isothermal adsorption curves. To investigate the surface chemistry, Fourier transform infrared spectrometer (FT-IR), X-ray spectroscopy (XPS), Scanning electron microscopy (SEM), and X-ray diffraction (XRD) were carried out. The pyrolysis and pore-forming mechanisms were demonstrated by TG-FTIR obtained at different temperatures and XRD patterns of unwashed samples. The materials were also applied as toluene adsorbents. The dynamic adsorption breakthrough curves of different samples were determined on a self-made adsorption system and fitted by the Yoon-Nelson model. The mass transfer behaviors were analyzed by the fitting results. The regeneration performances of selected samples were tested for more than four runs. The results of this work indicated that efficient toluene adsorbents could be prepared from direct pyrolysis of appropriate food waste components. The selected food waste components had the potential for mass-production of high-quality carbonaceous materials.

2. Materials and methods

2.1. Synthesis of N-doped hierarchical porous carbons

The bones, crab shells, and shrimp shells used in this work were bought in local markets. The results of those components' proximate analysis and ultimate analysis were shown in Table S1. All raw materials were washed and crashed into powders for further usage. The purified powder was placed in a quartz tube and heated to the set temperatures (400 °C, 700 °C, 800 °C, and 900 °C) with a heating rate of 10 °C/min to obtain self-activated biochar (Caˆndido et al., 2020, Sun et al., 2017). All samples were kept at the set temperature for 90 min for higher biochar production (Tripathi et al., 2016). The pyrolyzed samples were cooled to room temperature and soaked in plenty of 2 mol/L HNO_3 for 24 h. The soaked powders were washed with deionized water repeatedly. The washed samples were dried at 105 °C in the oven overnight and labeled as BC, CC, and SC-X (X = 400,700,800, and 900 °C) according to different raw materials and synthesis temperatures. The pyrolysis processes and gaseous products were analyzed by the TG-FTIR experiments. The TG experiments were carried out on a thermogravimetric analyzer (Netzsch, STA 449 F3, German). About 10 mg of raw materials were placed in a crucible. The samples were heated from room temperature to 1000 °C with a heating rate of 10 °C/min in a pure argon gas atmosphere. The gaseous products were inlet into an FT-IR analyzer (Tensor 27, Bruker, German). The temperature of the sample cell was set at 200 °C. The scan rate was set as 16 times/s. The spectra were scanned in the range of 4000 cm^{-1} to 650 cm^{-1} with a resolution of 4 cm^{-1}.

2.2. Material characterizations

The porous structure of BCs, CCs, and SCs were analyzed using their nitrogen sorption isotherms at 77 K. The specific data were obtained on a

gas sorption analyzer (Micromertics, ASAP 2460, USA). Before the adsorption tests, all samples were heated up to 300 °C and kept for 8 h to remove all contained impurities and moisture. The surface functional groups were determined by FT-IR and XPS spectra. The FT-IR spectra of different materials ranging from 400 cm^{-1} to 4000 cm^{-1} with a resolution of 4 cm^{-1} were obtained on a FTIR Spectrometer (Nicolet is50, Thermo Fisher, USA). The XPS spectra of BCs, CCs, and SCs were obtained on a Thermo Scientific K-Alpha (Thermofisher, USA). The wide scan survey and high solution survey of C1s, O1s, and N1s were all obtained. The SEM images of samples were captured on a field emission scanning electron microscope (SU8010, Hitachi, Japan). The XRD patterns of different samples were scanned in the range of 10°–80° with X'pert3 Powder (Malvern Panalytical, UK).

3. Results and discussion

3.1. The pyrolysis behaviors of different food waste components

To study the pyrolysis behaviors of different components, thermogravimetric tests were carried out. The TG curves of bone, crab shell, and shrimp shell were shown in Fig. 1 (a), (b), and (c), respectively. Results showed that all three raw materials had a weight loss process ranged from 200 °C to 400 °C. The weight loss peaks of the crab shell and shrimps shell consisted of two continuous weight loss peaks, which indicated the decomposition of chitin and protein, respectively. For bone, only one broad weight loss peak occurred in this stage. With the increment of temperature, crab shell and shrimp shell showed another weight loss peak around 700 °C. This peak indicated the decomposition of calcite (Zhang et al., 2019). For bone, the subsequent weight loss which can be attributed to the decomposition of hydroxyapatite happened between 700 °C and 900 °C (Kaseva, 2006; Niu et al., 2017). The char yields obtained in fixed bed pyrolysis were shown in Fig. 1(d). BCs showed the lowest final product yields among all samples due to the highest ash content. The final product yields of all samples were less than 10%, which proved the presence of the self-activation process.

The TG-FTIR spectrum obtained from different conditions demonstrated the gaseous pyrolysis products from different stocks. The three-dimensional TG-FTIR spectra of bone, crab shell, and shrimp shell were shown in Fig. 1 (e), (f), and (g), respectively. Consistent with the TG results, the adsorption peaks mainly appeared on the temperature ranges of 200 °C-400 °C and 700 °C-900 °C. The FT-IR spectra obtained at selected temperatures were shown in Fig. S1. From the spectra can be seen that the species of gaseous pyrolysis products generated at the first weight-loss stage were more complicated than those generated at 700 °C-900 °C. Fig. S1 (a), (b), and (c) demonstrated the spectrum obtained at 300 °C, 325 °C, 350 °C, 375 °C, and 400 °C, respectively. For all three raw materials, the spectrum generated at 350 °C showed the strongest absorbance. The gaseous products mainly included NH_3 (966 cm^{-1}), C-O groups (alcohols, phenols, and esters, 950 cm^{-1}-1300 cm^{-1}), aromatic compounds (1420 cm^{-1} -1600 cm^{-1}), C═O groups (ketones, aldehydes, carboxylic acids, primary amides, and esters, 1600 cm^{-1} -1850 cm^{-1}), CO_2 (2240 cm^{-1} -2400 cm^{-1}), hydrocarbons (2850 cm^{-1}-3100 cm^{-1}), –OH groups (H_2O, alcohols, and phenols, 3430 cm^{-1}), and water vapor (3500 cm^{-1}-3950 cm^{-1}) (Liang et al., 2018). The spectra obtained from 700 °C to 900 °C were relatively simple. Fig. S1 (d), (e), and (f) showed the spectra which only contained the adsorption peaks of CO, CO_2, and H_2O. Fig. S2 showed emission intensity of different gaseous produced from the pyrolysis process of different components under the temperature range of 300 °C to 400 °C. Results showed that NH_3 and CO_2 were the main gaseous products in this stage. CO_2 was produced from the dehydration in the carboxyl group of amino acids and the decarboxylation of side chains of amino acids and the reforming of carboxyl groups (Wei et al., 2018). In chitin, CO_2 was chiefly derived from the further cleavage of the C-O-C bonds after the glycosidic bonds were destroyed (P. Zhang et al., 2019). NH_3 was mainly produced from the cracking of protein. During the cracking process, peptide-bond were destroyed into linear amide and cyclic amide. NH_3 was generated during the decomposition of amides (Tian et al., 2013).

The evolution characteristics of CO_2, aromatic compounds, and compounds containing C═O groups such as ketones, aldehydes, carboxylic acids were pretty similar. From 300 °C to 350 °C, the emission intensities of these gases were improved with the increment of temperature. When the temperature continued to rise, the emission intensities decreased. This result was consistent with the trend of weight

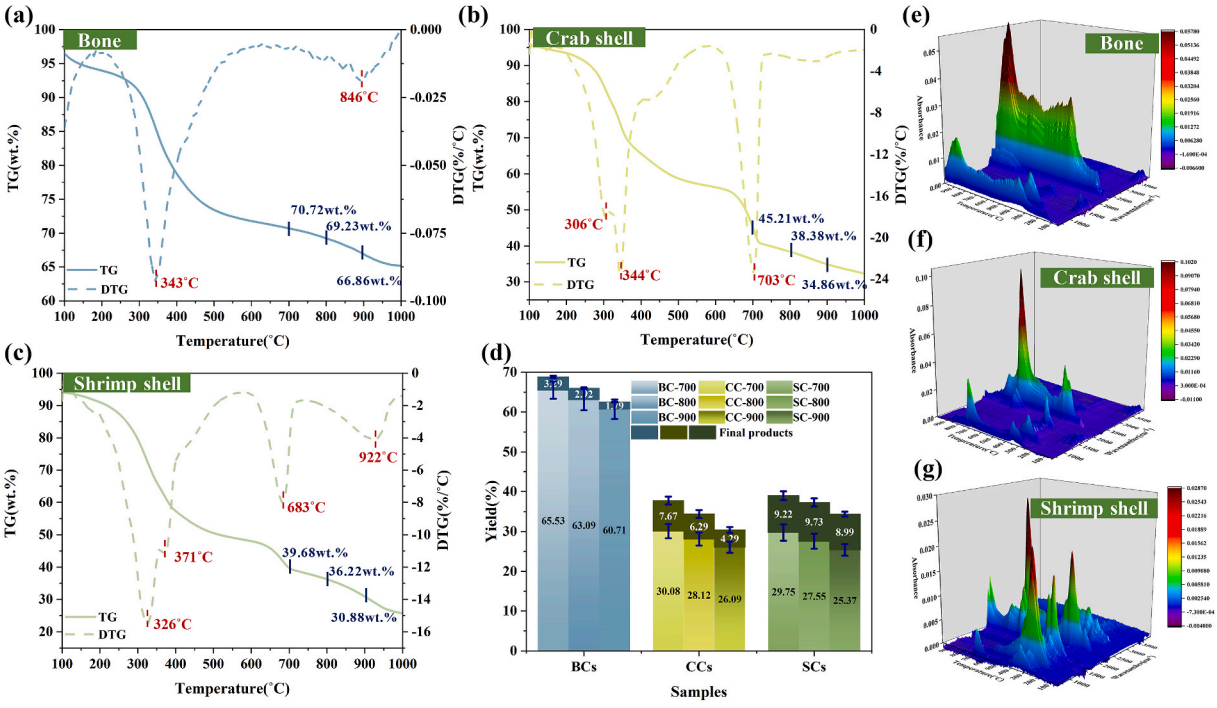

Fig. 1. Thermogravimetric behaviors and fix bed pyrolysis yields of different samples: thermogravimetric curves of: (a) bone, (b) crab shell, and (c) shrimp shell, (d) carbon yield of fix bed pyrolysis process, and 3D FT-IR spectra of different temperature of: (e) bone, (f) crab shell, and (g) shrimp shell.

loss rate. Similar trends indicated that all those gaseous products were generated from the same cracking reactions. Besides, the absorbance of NH_3 and compounds containing C-O groups such as phenols showed the same changing trends with the increment of temperature. The intensities increased before 320 °C and then decreased continuously.

3.2. Characterization of hierarchical porous carbons

3.2.1. Structures of hierarchical porous carbons

The N_2 isothermal adsorption curves and pore size distribution of BC-900, CC-900, and SC-900 were shown in Fig. 2 (a) and (b), respectively. The N_2 isothermal adsorption curves of all three samples exhibited the combined characteristics of type I and IV isothermal adsorption curves. Type I characteristics and type IV characteristics proved the presence of micropore and mesopore, respectively. BC-900 owned the highest specific surface area (1405.06 m^2/g) and total pore volume (0.97 cm^3/g) among all samples. The shape of sorption hysteresis of BC-900 also differed from that of CC-900 and SC-900, which indicated the different pore structures between different samples. CC-900 and SC-900 showed pretty similar structures. The rising trend was observed when $P/P_0 > 0.9$ indicated the presence of macropores. CC-900 obtained a larger total pore volume than SC-900 due to higher macropore volume. For the pore size distribution of different samples, BC-900 had more pores than CC-900 and SC-900 for the pore size range from 0 to 10 nm. Abundant micropores with pore widths of 0.68 nm and 1.27 nm existed in three samples. These micropores provided the main adsorption sites during the dynamic adsorption process of VOCs at low concentrations (Liu et al., 2020). Besides, all samples also had a large content of mesopores with pore width ranged from 2 nm to 4 nm. Mesopores can effectively enhance the mass transfer process (Hyun et al., 2020) and provide additional adsorption sites under high adsorbent concentration conditions (Liu et al., 2020).

The pyrolysis temperature also had an exclusive influence on the porous structure of different samples. For CCs and SCs, the specific surface area was improved with the increment of pyrolysis temperature. The specific surface area and other structural parameters were shown in Table S2. The pore size distribution of BCs, CCs, and SCs was shown in Fig.S3 (a), (b), and (c), respectively. CCs and SCs obtained similar structures for the same source of activation agent and template. The hierarchical porous structure of BCs was developed with the increment of pyrolysis temperature.

3.2.2. Surface chemistry of hierarchical porous carbons

The functional groups distributed on the surfaces of hierarchical porous carbon were determined by FT-IR and XPS. The FT-IR spectra of different samples were shown in Fig. S4. For all samples, the spectra could be divided into two major fingerprint regions. The O-H stretching represented by a broad peak ranged from 3300 cm^{-1} to 3600 cm^{-1} indicated the presence of –OH groups (polymeric –OH). For another fingerprint region, two broad peaks ranged from 900 cm^{-1} to 1300 cm^{-1} and 1400 cm^{-1} to 1600 cm^{-1} respectively included the adsorption peaks of C-H deformation (aromatics), C-O stretching (alcohols, esters, and ethers), C-H stretching (aromatics), C-H deformation (alkanes), and C═C ring stretching (aromatics) (Aboulkas et al., 2017).

The quantitative element distribution and binding chemistry were determined by XPS. The XPS wide scan spectra of different samples were shown in Fig. S5. According to the XPS wide scan results, only three peaks (C1s peak, O1s peak, and N1s peak) appeared in the samples. The C1s surveys of different samples showed in Fig. S6 was fitted by four different peaks (284.5 eV (C-C groups), 285.4 eV (C-O groups),286.5 eV (C═O groups), and 288.4 eV (O-C═O groups)) (Wang et al., 2020). Results showed that C-O groups (alcohols, phenols, or esters) and C═O groups (carbonyl groups) were less distributed on the surfaces. The peak indicated graphitized carbon occupied the most prominent peak area among all four peaks. Abundant oxygen-containing surface functional groups can be beneficial for the adsorption of VOCs by enhancing the

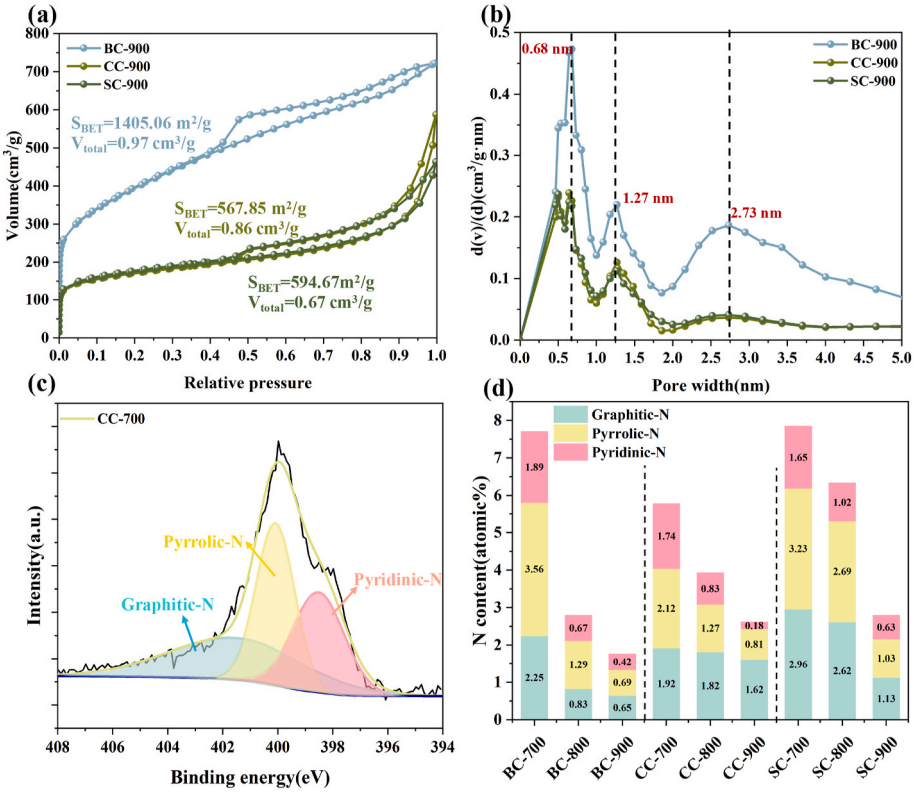

Fig. 2. Structural properties and surface chemistry of hierarchical porous carbon: (a) N_2 isothermal adsorption curves of BC-900, CC-900, and SC-900, (b) pore size distribution of BC-900, CC-900, and SC-900, (c) N1s survey of CC-700, and (d) nitrogen-containing surface functional groups' distribution of different samples.

interactions between VOCs molecules and adsorbents (Meng et al., 2019). N-containing surface functional groups can effectively facilitate interactions between VOCs molecules and adsorbents by accelerating the polarization of π electrons (Du et al., 2020). The pyrrolic-N functional groups had the best adsorption affinity with toluene among all N-containing functional groups by boosting the π-π dispersive interaction with the aromatic ring (Su et al., 2020). According to BC, CC, and SC-700 obtained enriched N-containing surface functional groups from the pyrolysis process of chitin and protein. The nitrogen content of BC, CC, and SC-700 were 7.7%, 5.78%, and 7.84% respectively. With the increment of pyrolysis temperature, surface N-containing groups were converted into gas and tar. For BC, CC, and SC-900, the N contents decreased to 1.76%, 2.61%, and 2.79%, respectively. The N1s spectrum of different samples was fitted by three different peaks (398.5 eV (Pyridinic N), 400.1 eV (Pyrrolic N), and 401.5 eV (Graphitic N)) (Chen et al., 2021). The N1s surveys of different samples were shown in Fig. S7. The relative contents of different N-containing surface functional groups were determined by the fitted peak area. The results of N-containing surface functional groups' distributions for different samples were shown in Fig. 2 (d). For BCs, CCs, and SCs, the pyrrolic-N and graphitic-N were the main components of N-containing functional groups. Therefore, during the adsorption process, the material surfaces had strong affinities with toluene molecules. The materials were appropriate toluene adsorbents.

3.2.3. Surface morphology and texture

The morphologies of BCs, CCs, and SCs were showed in Fig. 3. For BCs, pores in irregular shapes occurred on the surfaces. During the high-temperature pyrolysis process, hydroxyapatite started to decompose. CO_2 and H_2O generated during the decomposition process reacted with the surface carbon layer. With the increase of pyrolysis temperature, the surface of the material was broken continuously. The highly porous structure of BC-900 was shown in Fig. 3 (c). CCs exhibited complex crosslinked network structures. Crab shell-based biochar's stacked-layer structure was reported in previous literature (Dai et al., 2017). After self-activation and acid etching, the original smooth layer structure was transformed into a uniform 3D-honeycomb-like interconnected network structure (Li et al., 2018). The 3D network structure could provide transfer channels for adsorbate molecules during the adsorption process. From Fig. 3 (f) can be seen that SC-700 owned a smooth layer structure with some wrinkles and pores and distributed on the surface. With the increment of pyrolysis temperature, more and more fractured wrinkle structures appeared on the surface. When the pyrolysis temperature was raised to 900 °C, a large number of pores appeared on the surface of the material.

3.2.4. Hierarchical porous structure forming mechanisms

According to the gravimetric results of bone, crab shell, and shrimp shell, after the decomposition of protein and chitin, weight loss continued with the increment of temperature. The next weight-loss stage occurred at the temperature range of 700 °C-900 °C. During that weight-loss stage of different stocks, CO_2 was still one of the major gaseous products. In this stage, CO also started to occur from the reaction between CO_2 and solid residues. Fig. 4 (a), (b), and (c) showed the emission intensities' changing trend of CO_2, CO, and H_2O, respectively. For crab shells, the emission intensities of CO and CO_2 increased at first, reached the highest value at 706.4 °C, and then started to decrease. A similar trend with the increment of the temperature of CO and CO_2 proved the CO_2 self-activation mechanism. Meanwhile, H_2O was also generated from the degradation of macromolecular substances. Under high-temperature conditions, H_2O reacted with carbon as an activation agent to create more micropores.

The emission of CO_2 had an exclusive influence on the materials' structures. The N_2 isothermal adsorption curves of different materials were shown in Fig. 4 (d), (e), and (f), respectively. For bone, the CO_2 emission got an enhancement above 800 °C, which developed the porous structure of BC-900. The CO_2 emission of crab shells mainly happened below 750 °C, which resulted in similar structures of CC-700, 800, and 900. For shrimp shells, another emission peak of CO occurred between 750 °C and 800 °C, which improved the specific area of SC-800.

The weight loss was caused by the decomposition of inorganic salts embed in the samples. To investigate the transformation process of those inorganic salts, the XRD patterns of unwashed samples prepared at different temperatures were shown in Fig. 4 (g), (h), and (i). For BCs, the XRD patterns didn't change significantly with the increment of preparation temperature. The main inorganic salt components in BCs were hydroxyapatite. With the increment of preparation temperature, the width of peaks decreased. The results indicated that the crystallinity of hydroxyapatite increased (Alkurdi et al., 2020). For CC-400 and SC-400, the existing forms of inorganic salts were mainly $CaCO_3$. After pyrolyzed

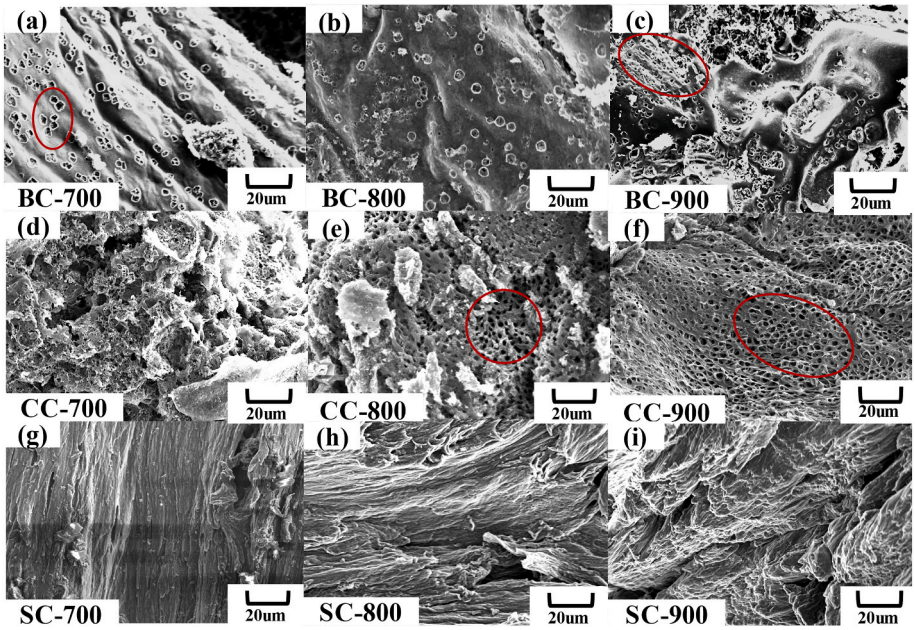

Fig. 3. SEM images of different samples: (a) BC-700, (b) BC-800, (c) BC-900, (d) CC-700, (e) CC-800, (f) CC-900, (g) SC-700, (h) SC-800, and (i) SC-900.

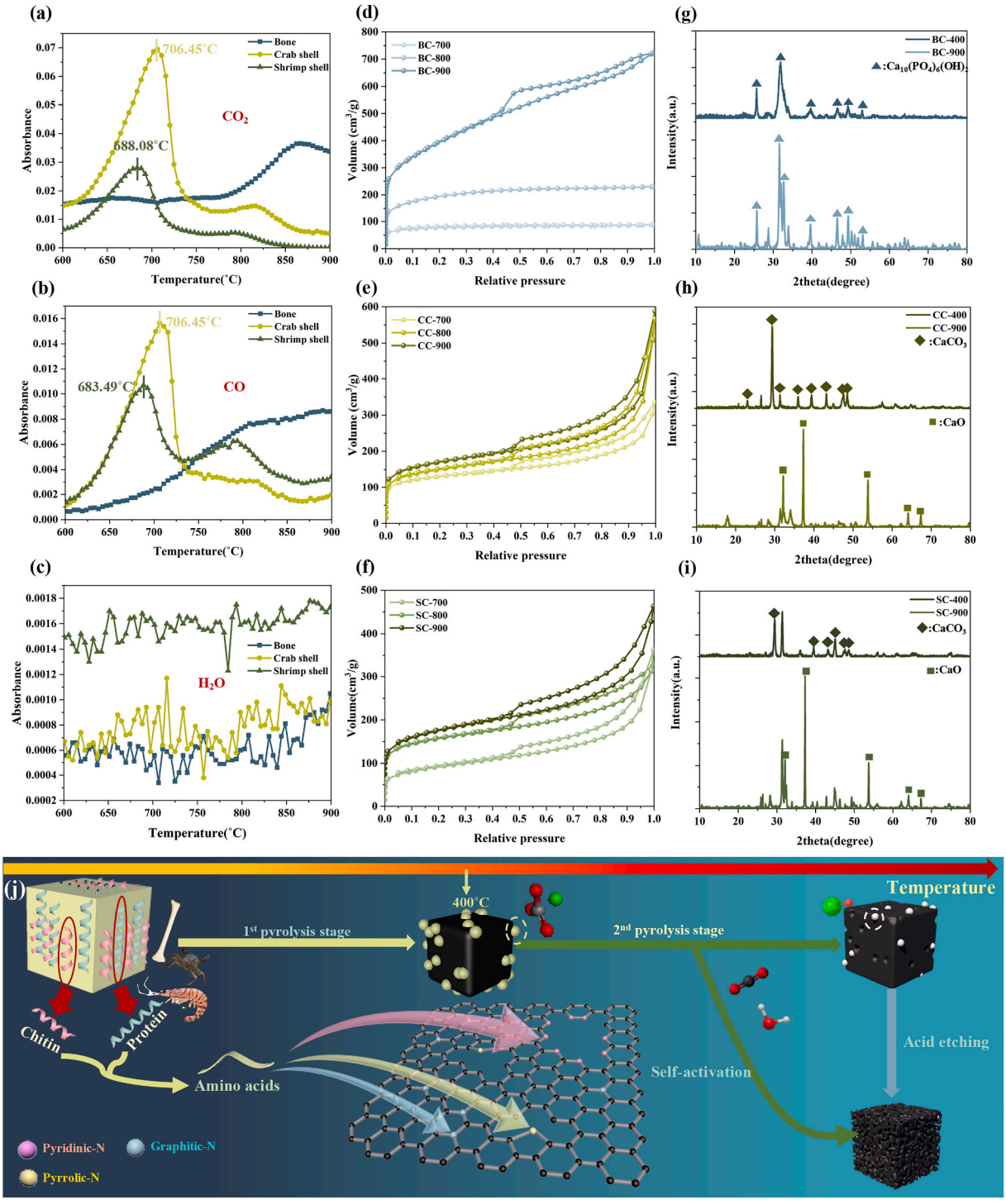

Fig. 4. Hierarchical porous structure forming mechanism: evolution intensities of different gaseous products from 600 °C to 900 °C: (a) CO_2, (b) H_2O, and (c) CO, N_2 isothermal adsorption curves of different samples: (d) BCs, (e) CCs, and (f) SCs, XRD patterns of unwashed samples prepared at different temperatures: (g) BCs and (h) CCs, and (i) SCs, and (j) schematic mechanisms of hierarchical porous structure forming process.

at a higher temperature, $CaCO_3$ started to decompose into CaO and CO_2. The XRD patterns of all unwashed samples were shown in Fig. S8. CaO played the role of template, and CO_2 reacted with the pyrolyzed carbon as an activation agent.

The self-activation, templated, and N-doping mechanisms was shown in Fig. 4 (j). Pyridinic-N and pyrrolic-N mainly came from the direct cyclization reactions of amino acids. Meanwhile, graphitized-N was formed through ring condensation reactions of pyridinic-N. With the increment of preparation temperature, the strong secondary reactions of amino acids could also form pyridinic-N and pyrrolic-N (Chen et al., 2017). The decomposition of inorganic salts and pyrolysis of chitin and protein provided the activation agents and templates simultaneously. The N-doped hierarchical porous carbon was successfully prepared by facile pyrolysis of the selected raw materials.

3.3. VOCs adsorption potential of different materials

To investigate the hierarchical porous carbons' potential as VOCs

adsorbents, the dynamic toluene adsorption breakthrough curves of different samples were shown in Fig. 5 (a), (b), and (c). Results showed that hierarchical porous carbons derived from the direct pyrolysis process of different food waste components had satisfying toluene adsorption capacities. For materials prepared from the same component, higher preparation temperature can effectively improve the toluene adsorption capacity by creating a more developed porous structure. The specific toluene adsorption properties were shown in Table 1. BC-900 had the highest adsorption capacity of 288.12 mg/g among all samples, superior to other reported solid wastes-based chemically activated carbon. Other non-activated biochars were also listed to compare with hierarchical porous biochar reported in this work (Rajabi et al., 2021) (Table S3). The results showed that hierarchical porous biochar prepared at higher temperatures performed superior toluene removal capacity to normal non-activated biochar due to its larger specific surface area. CC-900 and SC-900 also had promising toluene adsorption capacities of 157.51 mg/g and 165.69 mg/g, respectively. BC-700 showed the lowest adsorption capacity of 80.2 mg/g due to the limited specific surface area. The toluene adsorption capacities of carbonaceous

Table 1
Toluene adsorption properties and Y-N model fitting parameters of different samples.

Samples	Adsorption properties				Y-N model fitting parameters	
	$T_{0.05}$(min)	$T_{0.5}$(min)	$T_{0.9}$(min)	Q (mg/g)	k (min^{-1})	R^2
BC-400	–	–	–	2.12	–	–
BC-700	8	24	44	80.2	0.128	0.9884
BC-800	26	44	66	167.14	0.119	0.9885
BC-900	44	58	72	288.12	0.189	0.9962
CC-400	–	–	–	4.17	–	–
CC-700	24	38	48	124.17	0.186	0.9881
CC-800	26	38	48	145.47	0.232	0.9945
CC-900	30	40	48	157.61	0.241	0.9942
SC-400	–	–	–	3.26	–	–
SC-700	16	28	36	99.34	0.232	0.9844
SC-800	22	38	50	145.91	0.161	0.9859
SC-900	30	42	48	165.69	0.284	0.9841

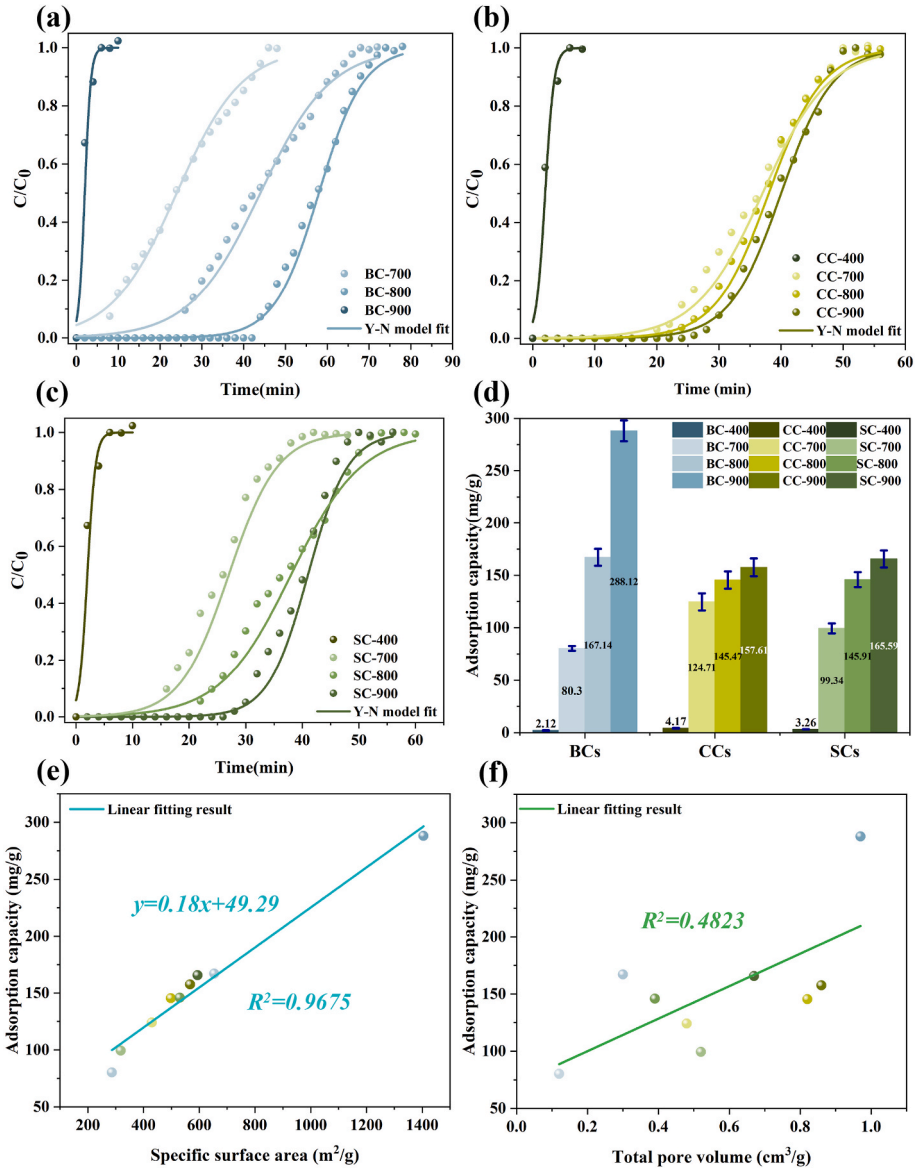

Fig. 5. Dynamic adsorption performances of different samples: adsorption breakthrough curves of: (a) BCs, (b) CCs, and (c) SCs and (d) adsorption capacities of toluene for different samples and relationships between adsorption capacities and different structural parameters: (e) specific surface area, and (f) the total pore volume.

materials derived from normal temperature-pyrolysis (BC, CC, and SC-400) were also determined. The results showed that these materials showed poor adsorption performance for toluene. All adsorption processes were completed within 10 min. The adsorption capacities were all less than 10 mg/g. The results indicated that micropores generated from the high-temperature pyrolysis process provided sufficient adsorption sites for toluene. To study the relationship between the adsorption performances and structural parameters, the adsorption capacities were linear fitted with the specific surface areas and the total pore volumes of the biochar. The fitting results were shown in Fig. 5 (e) and (f), respectively. Results showed that a strong positive correlation (R^2 = 0.9675) existed between the adsorption capacity and the specific surface area. The total pore volume didn't show an obvious influence on the adsorption performance. Similar results were reported by previous literature (X. Zhang et al., 2019).

For the mass transfer behaviors of different samples, the mass transfer process durations of BCs were longer than that of CCs and SCs. For BC-900, the duration was 28 min. CC-900 and SC-900 had shorter duration of 18 min, which was caused by better mass transfer abilities. The specific mass transfer processes on different samples were evaluated by the Yoon-Nelson model fitting results. The Yoon-Nelson model was shown as follows (Chen et al., 2019):

$$t = \tau + \frac{1}{k} ln \frac{C_t}{C_0 - C_t},$$

where τ was the time when the outlet concentration reaches half the initial concentration, k is the adsorption rate parameter, which could partially reflect the diffusion and mass transfer resistance, and C_0 and C_t represent the initial and outlet concentration, respectively, at time t.

The adsorption rate k of CCs and SCs was higher than that of BCs (0.119–0.189 min^{-1}) due to the 'micropore-mesopore-macropore' hierarchical porous structure. SC-900 had the highest k of 0.284 min^{-1} among all the samples. Mesopores and macropores had a positive influence on the adsorption rate by providing mass transfer channels (Zhu et al., 2020). The changing trend of BCs' adsorption rate parameter clearly reflected the influence of mesopores. The adsorption rate parameter k of BC-900 was effectively improved from 0.119 min^{-1} to 0.189 min^{-1} due to the plenty of mesopores generated above 800 °C.

Considering both adsorption amount and adsorption rate, BC-900 was the most appropriate toluene adsorbent. Abundant micropores provided adsorption sites and hierarchical porous structures that were obtained under high-temperature conditions played the role of mass transfer channels. BC-900 could realize the rapid and efficient removal of toluene.

3.4. Thermal regeneration performances of hierarchical porous carbon

To study thermal regeneration performances of three different hierarchical porous carbon samples. All three samples were kept at 300 °C for 1 h to desorb the absorbed toluene molecules. The 'adsorption-desorption' cycles of different samples were shown in Fig. 6 (a), (b), and (c) respectively. From the breakthrough curves of different cycles can be seen that the adsorption performances before and after the regeneration processes were similar, which indicated that regeneration recovered the adsorption capacities effectively. Fig. 6(d) showed the adsorption capacities and regeneration efficiencies after several 'adsorption-desorption' cycles. Results showed that after three 'adsorption-desorption' cycles, BC-900, CC-900, and SC-900 remain 86.2%, 87.4%, and 84.8% of the original adsorption capacities.

4. Limitations and challenges

For biochar's application in VOCs removal, some limitations and challenges remained. The following points should be considered:

(1) Compared to some high-quality chemical-modified (activated) carbon-based materials (Dai et al., 2017; Pi et al., 2021), the specific surface area and total pore volume were limited. The activation agent (CO_2 and H_2O) provided by the raw material was not enough to create plenty of micropores as chemical activation

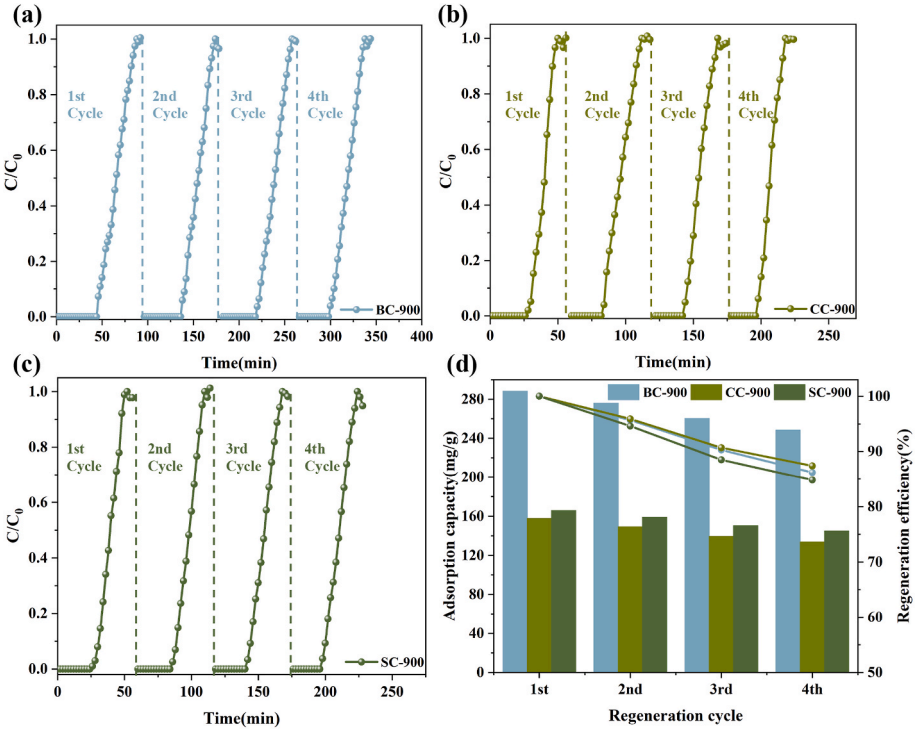

Fig. 6. Regeneration performances of different samples: adsorption breakthrough curves of different regeneration cycles: (a) BC-900, (b) CC-900, and (c) SC-900 and (d) toluene adsorption capacities of different samples for different regeneration cycle.

agent (KOH, H_3PO_4, etc.). More appropriated raw materials and suitable pyrolysis conditions need to be explored.

(2) The regeneration performances of biochar were not satisfying enough compared to some other reported carbon-based materials (Xu et al., 2021; Yang et al., 2021). A more efficient regeneration method should be utilized.

5. Conclusions

In this work, N-doped hierarchical porous carbons were successfully prepared from direct pyrolysis of three food waste components (bone, crab shell, and shrimp shell). The pyrolysis process can be divided into two stages: pyrolysis of chitin and protein, and thermal decomposition of inorganic salts. During the pyrolysis of chitin and protein, a great variety of gaseous products, including CO_2 and H_2O generated. CO occurred when inorganic salts started to decompose with the increment of pyrolysis temperature. The generation of CO_2 directly influenced the materials' structures. The materials obtained high specific surface area (1405.06 m^2/g), large total pore volume (0.97 cm^3/g), and hierarchical porous structure. The inorganic salts serve as the pore template and activation agent source which leaded to the hierarchical porous structure left in the derived biochar. The N-doped hierarchical porous carbon showed satisfying adsorption capacity (288.12 mg/g) and rapid adsorption process ($k = 0.284\ min^{-1}$) for toluene. The materials also can be repeatedly used for several 'adsorption-desorption' cycles and remain promising adsorption capacities (84.8%–87.4% of the original adsorption capacities). Results of this work provided a facial and low-cost preparation method for the mass production of N-doped hierarchical porous carbon, which can be utilized as efficient and circulated VOCs adsorbent.

Credit author statement

Yuxuan Yang: Conceptualization , Methodology , Investigation , Data curation, Writing - Original Draft: Chen Sun: Formal analysis, Methodology: Qunxing Huang: Supervision and Writing- Original Draft: Jianhua Yan: Supervision.

Declaration of competing interest

The authors declare that they have no known competing financial interests or personal relationships that could have appeared to influence the work reported in this paper.

Acknowledgment

This work was supported by the National Key Research and Development Program of China (2018YFC1901300) and Key Research and Development Program of Shandong province (2019JZZY020806).

Appendix A. Supplementary data

Supplementary data to this article can be found online at https://doi.org/10.1016/j.chemosphere.2021.132702.

References

Aboulkas, A., Hammani, H., El Achaby, M., Bilal, E., Barakat, A., El harfi, K., 2017. Valorization of algal waste via pyrolysis in a fixed-bed reactor: production and characterization of bio-oil and bio-char. Bioresour. Technol. 243, 400–408.

Alkurdi, S.S.A., Al-Juboori, R.A., Bundschuh, J., Bowtell, L., McKnight, S., 2020. Effect of pyrolysis conditions on bone char characterization and its ability for arsenic and fluoride removal. Environ. Pollut. 262 (September 2018), 114221.

Bedane, A.H., Guo, T.X., Eić, M., Xiao, H., 2019. Adsorption of volatile organic compounds on peanut shell activated carbon. Can. J. Chem. Eng. 97 (1), 238–246.

Bommier, C., Xu, R., Wang, W., Wang, X., Wen, D., Lu, J., Ji, X., 2015. Self-activation of cellulose: a new preparation methodology for activated carbon electrodes in electrochemical capacitors. Nano Energy 13, 709–717.

Ca Ndido, N.R., Prauchner, M.J., Vilela, A.D.O., Pasa, V.N.M.D., 2020. The use of gases generated from eucalyptus carbonization as activating agent to produce activated carbon: an integrated process. J. Environ. Chem. Eng. 8 (4), 103925.

Chabot, V., Higgins, D., Yu, A., Xiao, X., Chen, Z., Zhang, J., 2014. A review of graphene and graphene oxide sponge: material synthesis and applications to energy and the environment. Energy Environ. Sci. 7 (5), 1564–1596.

Chen, L., Yuan, J., Li, T., Jiang, X., Ma, S., Cen, W., Jiang, W., 2021. A regenerable N-rich hierarchical porous carbon synthesized from waste biomass for H2S removal at room temperature. Sci. Total Environ. 768, 144452.

Chen, Q., Zhu, R., Deng, L., Ma, L., He, Q., Du, J., Fu, H., Zhang, J., Wang, A., 2019. One-pot synthesis of novel hierarchically porous and hydrophobic Si/SiOx composite from natural palygorskite for benzene adsorption. Chem. Eng. J. 378 (May), 122131.

Chen, W., Yang, H., Chen, Y., Xia, M., Chen, X., Chen, H., 2017. Transformation of nitrogen and evolution of N-containing species during algae pyrolysis. Environ. Sci. Technol. 51 (11), 6570–6579.

Crespo, D., Yang, R.T., 2006. Adsorption of organic vapors on single-walled carbon nanotubes. Ind. Eng. Chem. Res. 45 (16), 5524–5530.

Dai, L., Tan, F., Li, H., Zhu, N., He, M., Zhu, Q., Hu, G., Wang, L., Zhao, J., 2017. Calcium-rich biochar from the pyrolysis of crab shell for phosphorus removal. J. Environ. Manag. 198, 70–74.

Du, Y., Chen, H., Xu, X., Wang, C., Zhou, F., Zeng, Z., Zhang, W., Li, L., 2020. Surface modification of biomass derived toluene adsorbent: hierarchically porous characterization and heteroatom doped effect. Microporous Mesoporous Mater. 293 (October 2019), 109831.

Gao, F., Geng, C., Xiao, N., Qu, J., Qiu, J., 2018. Hierarchical porous carbon sheets derived from biomass containing an activation agent and in-built template for lithium-ion batteries. Carbon 139, 1085–1092.

Gao, M., Liu, W., Wang, H., Shao, X., Shi, A., An, X., Li, G., Nie, L., 2021. Emission factors and characteristics of volatile organic compounds (VOCs) from adhesive application in indoor decoration in China. Sci. Total Environ. 779, 145169.

Hyun, G., Song, J.T., Ahn, C., Ham, Y., Cho, D., Oh, J., Jeon, S., 2020. Hierarchically porous Au nanostructures with interconnected channels for efficient mass transport in electrocatalytic CO2 reduction. Proc. Natl. Acad. Sci. U. S. A 117 (11), 5680–5685.

Janus, R., Kuśtrowski, P., Dudek, B., Piwowarska, Z., Kochanowski, A., Michalik, M., Cool, P., 2011. Removal of methyl-ethyl ketone vapour on polyacrylonitrile-derived carbon/mesoporous silica nanocomposite adsorbents. Microporous Mesoporous Mater. 145 (1–3), 65–73.

Jin, Z., Wang, B., Ma, L., Fu, P., Xie, L., Jiang, X., Jiang, W., 2020. Air pre-oxidation induced high yield N-doped porous biochar for improving toluene adsorption. Chem. Eng. J. 385 (December 2019), 123843.

Kaseva, M.E., 2006. Optimization of regenerated bone char for fluoride removal in drinking water: a case study in Tanzania. J. Water Health 4 (1), 139–147.

Li, Y.F., Liu, Y.Z., Chen, S., Wang, P.F., Yuan, S.X., Li, X., Song, H., Chen, C.M., 2018. Self-templating synthesis nitrogen and sulfur co-doped hierarchical porous carbons derived from crab shells as a high-performance metal-free oxygen electroreduction catalyst. Mater. Today Energy 10, 388–395.

Li, Y., Jin, Y., Borrion, A., Li, H., 2019. Current status of food waste generation and management in China. Bioresour. Technol. 273 (August 2018), 654–665.

Liang, F., Wang, R., Hongzhong, X., Yang, X., Zhang, T., Hu, W., Mi, B., Liu, Z., 2018. Investigating pyrolysis characteristics of moso bamboo through TG-FTIR and Py-GC/MS. Bioresour. Technol. 256 (February), 53–60.

Liu, S., Peng, Y., Chen, J., Yan, T., Zhang, Y., Liu, J., Li, J., 2020. A new insight into adsorption state and mechanism of adsorbates in porous materials. J. Hazard. Mater. 382 (August 2019), 121103.

León, M., Marcilla, A.F., García, Á.N., 2019. Hydrothermal liquefaction (HTL) of animal by-products: influence of operating conditions. Waste Manag. 99, 49–59.

Lu, S., Huang, X., Tang, M., Peng, Y., Wang, S., Makwarimba, C.P., 2021. Synthesis of N-doped hierarchical porous carbon with excellent toluene adsorption properties and its activation mechanism. Environ. Pollut. 284, 117113.

Ma, X., Li, L., Zeng, Z., Chen, R., Wang, C., Zhou, K., Su, C., Li, H., 2019. Synthesis of nitrogen-rich nanoporous carbon materials with C3N-type from ZIF-8 for methanol adsorption. Chem. Eng. J. 363 (January), 49–56.

Meng, F., Song, M., Wei, Y., Wang, Y., 2019. The contribution of oxygen-containing functional groups to the gas-phase adsorption of volatile organic compounds with different polarities onto lignin-derived activated carbon fibers. Environ. Sci. Pollut. Control Ser. 26 (7), 7195–7204.

Nie, E., Zheng, G., Shao, Z., Yang, J., Chen, T., 2018. Emission characteristics and health risk assessment of volatile organic compounds produced during municipal solid waste composting. Waste Manag. 79, 188–195.

Niu, J., Shao, R., Liang, J., Dou, M., Li, Z., Huang, Y., Wang, F., 2017. Biomass-derived mesopore-dominant porous carbons with large specific surface area and high defect density as high performance electrode materials for Li-ion batteries and supercapacitors. Nano Energy 36 (February), 322–330.

Niu, J., Shao, R., Liu, M., Zan, Y., Dou, M., Liu, J., Zhang, Z., Huang, Y., Wang, F., 2019. Porous carbons derived from collagen-enriched biomass: tailored design, synthesis, and application in electrochemical energy storage and conversion. Adv. Funct. Mater. 29 (46), 1–23.

Pi, X., Qu, Z., Sun, F., Zhang, Z., Gao, J., 2021. Catalytic activation preparation of nitrogen-doped hierarchical porous biochar for efficient adsorption of dichloromethane and toluene. J. Anal. Appl. Pyrol. 156 (January), 105150.

Rajabi, H., Hadi Mosleh, M., Prakoso, T., Ghaemi, N., Mandal, P., Lea-Langton, A., Sedighi, M., 2021. Competitive adsorption of multicomponent volatile organic compounds on biochar. Chemosphere 283 (June), 131288.

Sharma, S., Thind, S.S., Kaur, A., 2015. In vitro meat production system: why and how? J. Food Sci. Technol. 52 (12), 7599–7607.

Su, C., Guo, Y., Chen, H., Zou, J., Zeng, Z., Li, L., 2020. VOCs adsorption of resin-based activated carbon and bamboo char: porous characterization and nitrogen-doped effect. Colloid. Surface. Physicochem. Eng. Aspect. 601 (May), 124983.
Sun, K., Leng, C.Y., Jiang, J.C., Bu, Q., Lin, G.F., Lu, X.C., Zhu, G.Z., 2017. Microporous activated carbons from coconut shells produced by self-activation using the pyrolysis gases produced from them, that have an excellent electric double layer performance. Xinxing Tan Cailiao/New Carbon Materials 32 (5), 451–459.
Sun, M.H., Huang, S.Z., Chen, L.H., Li, Y., Yang, X.Y., Yuan, Z.Y., Su, B.L., 2016. Applications of hierarchically structured porous materials from energy storage and conversion, catalysis, photocatalysis, adsorption, separation, and sensing to biomedicine. Chem. Soc. Rev. 45 (12), 3479–3563.
Tang, M., Huang, X., Peng, Y., Lu, S., 2020. Hierarchical porous carbon as a highly efficient adsorbent for toluene and benzene. Fuel 270 (September 2019), 117478.
Tian, Y., Zhang, J., Zuo, W., Chen, L., Cui, Y., Tan, T., 2013. Nitrogen conversion in relation to NH3 and HCN during microwave pyrolysis of sewage sludge. Environ. Sci. Technol. 47 (7), 3498–3505.
Tripathi, M., Sahu, J.N., Ganesan, P., 2016. Effect of process parameters on production of biochar from biomass waste through pyrolysis: a review. Renew. Sustain. Energy Rev. 55, 467–481.
Wang, A.Y., Sun, K., Wu, L., Wu, P., Zeng, W., Tian, Z., Huang, Q.X., 2020. Co-carbonization of biomass and oily sludge to prepare sulfamethoxazole super-adsorbent materials. Sci. Total Environ. 698, 134238.
Wei, X., Ma, X., Peng, X., Yao, Z., Yang, F., Dai, M., 2018. Journal of analytical and applied pyrolysis comparative investigation between co-pyrolysis characteristics of protein and carbohydrate by TG-FTIR and Py-GC/MS. J. Anal. Appl. Pyrol. 135 (381), 209–218.
Xiang, W., Zhang, X., Chen, K., Fang, J., He, F., Hu, X., Tsang, D.C.W., Ok, Y.S., Gao, B., 2020. Enhanced adsorption performance and governing mechanisms of ball-milled biochar for the removal of volatile organic compounds (VOCs). Chem. Eng. J. 385 (November 2019), 123842.
Xu, X., Guo, Y., Shi, R., Chen, H., Du, Y., Liu, B., Zeng, Z., Yin, Z., Li, L., 2021. Natural Honeycomb-like structure cork carbon with hierarchical Micro-Mesopores and N-containing functional groups for VOCs adsorption. Appl. Surf. Sci. 565 (March), 150550.
Yan, Y., Yang, C., Peng, L., Li, R., Bai, H., 2016. Emission characteristics of volatile organic compounds from coal-, coal gangue-, and biomass-fired power plants in China. Atmos. Environ. 143, 261–269.
Yang, Y., Sun, C., Lin, B., Huang, Q., 2020. Surface modified and activated waste bone char for rapid and efficient VOCs adsorption. Chemosphere 256, 127054.
Yang, Y., Lin, B., Sun, C., Tang, M., Lu, S., Huang, Q., Yan, J., 2021. Facile synthesis of tailored mesopore-enriched hierarchical porous carbon from food waste for rapid removal of aromatic VOCs. Sci. Total Environ. 773, 145453.
Zhang, P., Hu, H., Tang, H., Yang, Y., Liu, H., Lu, Q., Li, X., Worasuwannarak, N., Yao, H., 2019. In-depth experimental study of pyrolysis characteristics of raw and cooking treated shrimp shell samples. Renew. Energy 139, 730–738.
Zhang, X., Gao, B., Creamer, A.E., Cao, C., Li, Y., 2017. Adsorption of VOCs onto engineered carbon materials: a review. J. Hazard. Mater. 338, 102–123.
Zhang, X., Gao, B., Fang, J., Zou, W., Dong, L., Cao, C., Zhang, J., Li, Y., Wang, H., 2019. Chemically activated hydrochar as an effective adsorbent for volatile organic compounds (VOCs). Chemosphere 218, 680–686.
Zhu, L., Shen, D., Luo, K.H., 2020. A critical review on VOCs adsorption by different porous materials: species, mechanisms and modification methods. J. Hazard. Mater. 389 (January), 122102.